Three-dimensional Reconstruction of Thick Filaments from *Limulus* and Scorpion Muscle

MURRAY STEWART,*‡ ROBERT W. KENSLER,§ and RHEA J. C. LEVINE‡§
*Medical Research Council Laboratory of Molecular Biology, Cambridge, CB2 2QH, England;
‡Pennsylvania Muscle Institute, University of Pennsylvania Medical School, Philadelphia, Pennsylvania 19104; and §Department of Anatomy, Medical College of Pennsylvania, Philadelphia, Pennsylvania 19129

ABSTRACT We have produced three dimensional reconstructions, at a nominal resolution of 5 nm, of thick filaments from scorpion and *Limulus* skeletal muscle, both of which have a right-handed four-stranded helical arrangement of projecting subunits. In both reconstructions there was a distinct division of density within projecting subunits consistent with the presence of two myosin heads. Individual myosin heads appeared to be curved, with approximate dimensions of 16 × 5 × 5 nm and seemed more massive at one end. Our reconstructions were consistent with the two heads in a projecting subunit being arranged either antiparallel or parallel to each other and directed away from the bare zone. Although we cannot exclude the second of these interpretations, we favor the first as being more consistent with both filament models and also because it would enable easy phosphorylation of light chains. The antiparallel interpretation requires that the two heads within a subunit derive from different myosin molecules. In either interpretation, the two heads have different orientations relative to the thick filament shaft.

The thick filaments of invertebrate muscle are constructed from myosin arranged over an underlying core of paramyosin. The rodlike tails of the myosin molecules, together with paramyosin, make up the shaft of the filaments, whereas, in relaxed muscle, the globular myosin heads are arranged helically on the filament surface. During contraction these heads become attached to the thin, actin-containing filaments and form the cross-bridges that mediate the relative sliding of the interdigitating filament arrays.

x-ray diffraction studies (30–32) have indicated that the myosin heads in relaxed *Limulus* muscle are arranged on a helical lattice with 3N-fold screw symmetry and an axial spacing between cross-bridges of 14.5 nm. We have previously described protocols that permitted the relaxed structure to be preserved in thick filaments isolated from arthropod skeletal muscles (10). Electron micrographs of this material gave optical diffraction patterns and computed Fourier transforms that closely resembled the x-ray diffraction patterns of relaxed muscle (30–32). Analysis of these images by optical and computer methods demonstrated that, in filaments from the muscles of the horseshoe crab *Limulus polyphemus*, the tarantula, *Eurypelma* sp., and the scorpion *Vejovis spingera*, the myosin heads are arranged on a right-handed, four-stranded helical lattice (10, 11, 13, 16, 24). Our earlier studies, at a resolution of ~7 nm, also indicated that the projecting subunits on the *Limulus* filament surface were bent and elongated, approximately 20 × 8 × 8 nm and arranged at ~55° to the filament axis (24). We interpreted these projecting subunits to be the two heads of a myosin molecule, but we could not identify individual heads or specify their orientation. Furthermore, although thick filaments from a number of arthropod muscles all have the same helical arrangement of projecting subunits, they differ in both paramyosin content and shaft diameter (10, 13, 16). This raises the question of whether the detailed arrangement of myosin heads is similar in each filament.

In the present study we examined the three dimensional structure of thick filaments from the scorpion *Vejovis spinigera* and reinvestigated *Limulus* thick filaments at higher resolution. We employed a more sophisticated procedure of computer analysis that makes it possible to separate overlapping contributions on layer lines from terms deriving from Bessel functions of different order. In this way we have produced three-dimensional reconstructions of these filaments to nominal resolutions better than 5 nm, in which the distribution of density is consistent with the presence of two myosin heads in each projecting subunit. These reconstruc-

THE JOURNAL OF CELL BIOLOGY · VOLUME 101 AUGUST 1985 402-411

tions also contain information on the size, shape, and orientation of individual myosin heads.

MATERIALS AND METHODS

Thick filaments were isolated from whole tail muscles of the scorpion *Vejovis spinigera* by a modification of the technique of Hardwicke and Hanson (8) similar to that previously used to isolate *Limulus* and tarantula thick filaments (10, 16, 24), which is described in detail elsewhere (13). Specimens were negatively stained with 1% uranyl acetate as previously described (10) and examined with a JEOL 100S electron microscope at 80 kV with the anti-contamination device in operation. Electron micrographs of *Limulus* thick filaments were obtained as described (10). Optical diffraction was performed as previously described (10–12).

Images for computer processing were selected on the basis of the correspondence of their optical diffraction patterns to x-ray diffraction patterns from whole muscle (30–32) and the strength of high-frequency reflections. Micrographs were digitized at intervals corresponding to a spacing of ~1 nm on the original object. Fourier transforms were computed and layer-line data were obtained as described previously (12, 24). Terms on layer lines that derived from overlapping contributions from Bessel functions of different order were separated by least-squares analysis of a number of filaments that had different azimuthal rotations using software written by Dr. R. A. Crowther and described in detail elsewhere (2). Reconstructions produced by Fourier–Bessel inversion (3) were displayed either as contour plots or as pseudo-solid images using an AED 767 display terminal (AED Inc., Sunnyvale, CA) and software written by Drs. T. Horsnell, E. H. Egelman, and A. Lesk.

The distribution of stain around helical particles is usually not symmetrical. This may introduce small errors in the equator in computed Fourier transforms, so the radial variation of density in the reconstruction may not be strictly correct. In muscle thick filaments there is an additional problem related to their being composed of a dense central shaft surrounded by a halo of myosin heads. Since only information to a resolution of 5 nm was included in the syntheses, the boundary between shaft and heads was not clearly defined. Thus the density due to the heads becomes superimposed on a sloping background deriving from the shaft, and this could alter their detailed shape slightly in a radial direction. We circumvented these problems by omitting the equatorial data from the reconstruction, since the shaft contributes mainly to the equator whereas the major contribution from the heads is to the layer lines. However, removing the equator also omits from the synthesis any circumferentially averaged radial density variation associated with the heads. This is equivalent to assuming that the circumferentially averaged density due to the heads is constant in a radial direction. Although this assumption may not be strictly correct, it is unlikely to have altered the interpretation significantly. Nevertheless, we always compared reconstructions in which the equator was alternatively absent or present and only considered features that were present in both reconstructions as unlikely to be artifactual.

To establish molecular boundaries and to assess the significance of some features in the reconstructions, it was necessary to have an idea of the volume of myosin heads. The volume of individual vertebrate skeletal myosin S-1 heads, prepared by proteolysis, has been estimated at 151 nm^3 (18). This material contained a heavy chain of ~90,000 mol wt and two degraded light chains, so that its aggregate molecular weight was ~120,000 (giving a density of ~800 D/nm^3). Some material had probably been lost during proteolysis, and sequence studies (17) indicate that the heavy chain weight in an intact head is ~98,000 mol wt. This, with two light chains, would give an aggregate molecular weight of ~140,000, corresponding to a head volume of ~175 nm^3. However, because it has a grain size of ~2 nm, negative stain would be unlikely to outline the head exactly. This would be particularly so where the head was adjacent to the shaft and so the volume of a head outlined by negative stain would be larger. To compensate for this we used a volume of 250 nm^3, corresponding to a density of 500 D/nm^3, for the heads. To ensure that features seen in the reconstructions were not artifacts associated with this particular choice of volume, we also examined a range of head volumes and found that the overall interpretation was not very sensitive to this parameter.

RESULTS

Electron Micrographs of Scorpion and Limulus Thick Filaments

Fig. 1 illustrates typical electron micrographs of scorpion and *Limulus* thick filaments negatively stained with uranyl acetate. Both have very distinct repeating patterns, which, although similar, are not identical. The shaft diameter of *Limulus* filaments is ~24 nm (10), whereas that of scorpion is ~18 nm (13). Optical diffraction patterns (Fig. 2) of the two types of filament were also similar, with strong first and fourth layer lines together with a strong third layer line meridional intensity. These patterns closely resemble those obtained from relaxed whole muscle (30–32). We showed elsewhere (13, 24) that both filaments have a right-handed four-start helical surface lattice with a pitch of 174 nm, 12 times the 14.5 nm unit axial translation. Thus, the diffraction patterns represent sums of Bessel functions of order 0 and ±12N (N = 1, 2, 3, . . .) on layer lines that are a multiple of 3 and sums of Bessel functions of order 4N, where N is not a multiple of 3 (that is 1, 2, 4, . . .), on all other layer lines (see reference 14). Since there is substantial overlap between these Bessel function terms, reliable reconstructions to high resolution can only be obtained if contributions from terms deriving from different Bessel orders along each layer line are separated. We did not do this in our earlier low-resolution study and consequently obtained a view of only the overall shape of the projecting subunit (24) in which substructure was not well resolved. In the present study, we resolved Bessel terms with order up to ±16 by least-squares analysis of particles with different azimuthal orientations. Relative particle rotations were determined from the inner regions of the first and fourth layer lines (where there was negligible overlap of terms deriving from terms of different Bessel order), and, because there are 12 subunits per helical turn, these rotations were specified within the range 0 to 30°.

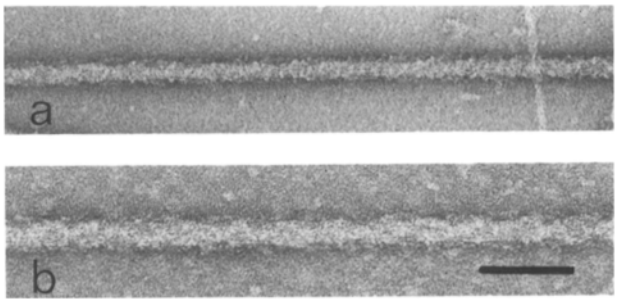

FIGURE 1 Typical electron micrograph of (*a*) scorpion and (*b*) *Limulus* thick filaments negatively stained with uranyl acetate. Bar, 100 nm. × 125,000.

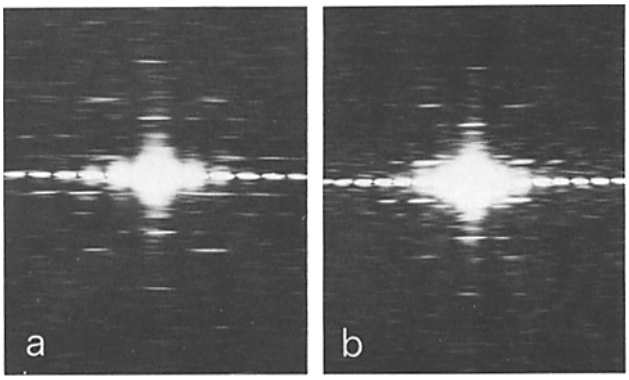

FIGURE 2 Optical diffraction patterns of (*a*) scorpion thick filament and (*b*) *Limulus* filament, showing strong first and fourth layer lines and a strong meridional reflection on the third layer line. Layer line spacing corresponds to 43.5 nm and the third layer line meridional reflection to 14.5 nm.

Three-dimensional Reconstruction of Scorpion Thick Filaments

Six filaments, selected on the basis of their optical diffraction patterns and that had relative orientations of 0, 2, 15, 17, 23, and 25°, were used to separate overlapping terms deriving from Bessel functions of different order on the equator and first nine layer lines. The least squares residual from this analysis represented 13.2% of the total intensity on layer lines 1 to 9, inclusive. (The least squares residual represented only 2% of the total intensity if the equator was included, but this was because all filaments were essentially cylindrical. We thought that the residual excluding the equator gave a better impression of reliability, since it was these data that were primarily responsible for the shape of the heads in the reconstructions.) The observation that 87% of the intensity was consistent with the final separation indicated a high degree of internal consistency in the data. Table I shows the terms extracted by this procedure and used in the reconstruction. Terms that represented <1% of total intensity and those in which the phase did not oscillate as expected (see reference 14) were rejected. Reliable data extended to ~0.25 nm^{-1} on layer lines 1 to 4 and to between 0.2 and 0.25 nm^{-1} on layer lines 5 to 9. Thus, data to a resolution of 4–5 nm were included in this synthesis. Terms that derived from Bessel functions of order 16 were the highest used in the reconstruction, and these corresponded to an azimuthal resolution of about 5.5 nm at the radius of the heads.

Figs. 3 and 4 show reconstructions obtained both with and without the contribution from the equator. The surfaces generated in these figures show the outline at a density corresponding to a head volume of ~250 nm^3 (or a density of 500 D/nm^3). Representations were also obtained at several other density levels, corresponding to a range of densities of 400 to 1,000 D/nm^3, and these showed essentially the same features, although naturally some of the more delicate aspects were less pronounced at higher density thresholds. In addition, inspection of contour plots of serial sections (axial, circumferential, and perpendicular to the axis) confirmed that the features identified were genuinely present in the reconstruction and were not artifacts associated with a particular density threshold. The slightly smaller size of the projecting subunits in the reconstruction containing the equator was a consequence of the general decrease in density with increasing radius associated with the equatorial data. This sloping background had the effect of increasing the size of the subunits at low radius (where they were partially obscured by the large density associated with the filament shaft) and decreasing their size at higher radii. It also slightly decreased their apparent radius in the reconstruction. However, detailed inspection of the two reconstructions indicated that the same major structural features were present in each.

Both reconstructions showed distinct helical ridges with a marked ziz-zag pattern made up of overlapping subunits projecting from the shaft. This closely resembled the pattern seen in shadowed filaments (11, 13). The projecting subunits in these ridges were oriented at ~55° to the filament axis, which corresponds to ~30° to the path of the 174 nm long-pitch helix. That the projecting subunits appeared to be composed of two lobes was most easily seen when the reconstructions were viewed at an angle to the filament axis (Fig. 4). The projecting subunit center of mass was at a radius of ~12.5 nm. Contour plots of cylindrical sections through the reconstruction (Fig. 5) showed clearly that the density in each projecting subunit was divided into two, with the lobe nearer the bare zone being stronger at higher radii whereas the lobe more distant from the bare zone was stronger at lower radii. Thus each subunit had two lobes located at slightly different radii with their centers of mass separated by ~5 nm. Although it was impossible to determine precise molecular boundaries, both lobes appeared elongated and had a narrow connecting density between projecting subunits. This connecting density was most easily seen when the equatorial data were omitted from the reconstruction, but was still present, as a surface protuberance, when these data were present (Figs. 3 and 4). The subunits in each reconstruction had an approximate two-fold axis or mirror line, which is most easily seen in Fig. 5 *b*.

TABLE I. *Contributions of Bessel Order N Used on Each Layer Line in the Thick Filament Reconstructions*

Layer line	Bessel order	
	Scorpion	*Limulus*
Equator	0, 12	0, 12
1	4, −8, 16	4, −8
2	−4, −16	−4, 8, −16
3	0, 12, −12	0, 12, −12
4	4, −8	4, −8, 16
5	—	−4, 8, −16
6	0	0, 12, −12
7	4, −8	4, −8
8	−4	−4, 8
9	0	0

Limulus Thick Filament Reconstruction

Figs. 3 and 4 show the reconstruction obtained from *Limulus* thick filaments. Seven filaments having relative orientations of 0, 1, 7, 8, 9, 16, and 29° were employed to separate overlapping Bessel terms, and the least squares residual for layer lines 1 to 9 represented 12.8% of the total layer line intensity. Thus, reconstructions using this data were comparable to those obtained on scorpion. Again, the nominal resolution was ~5 nm, although the quality of the higher frequency data appeared to be superior in the *Limulus* filaments and more higher-order Bessel terms were recovered. The present reconstruction was much superior to our earlier one (24) which extended to a resolution of only 7 nm and in which overlapping terms on layer lines were not separated. Table I lists the terms used for the synthesis.

The overall appearance of this reconstruction (Figs. 3 and 4) was similar to that obtained earlier (24) although more detail was present. The overlapping projecting subunits formed distinct ridges and each projecting subunit had a bilobed appearance. As observed previously (24), the general shape of the projecting subunits was elongated and curved, with the ends closer to the bare zone being less dense. In circumferential sections through the reconstruction (Fig. 5), the division into two major lobes was unmistakable, whereas our earlier, low-resolution study (24) had given little indication of this feature. As in the scorpion reconstructions, the lobe closer to the bare zone was stronger at higher radii, whereas the lobe more distant from the bare zone was stronger at lower radii. The two lobes in the *Limulus* reconstruction

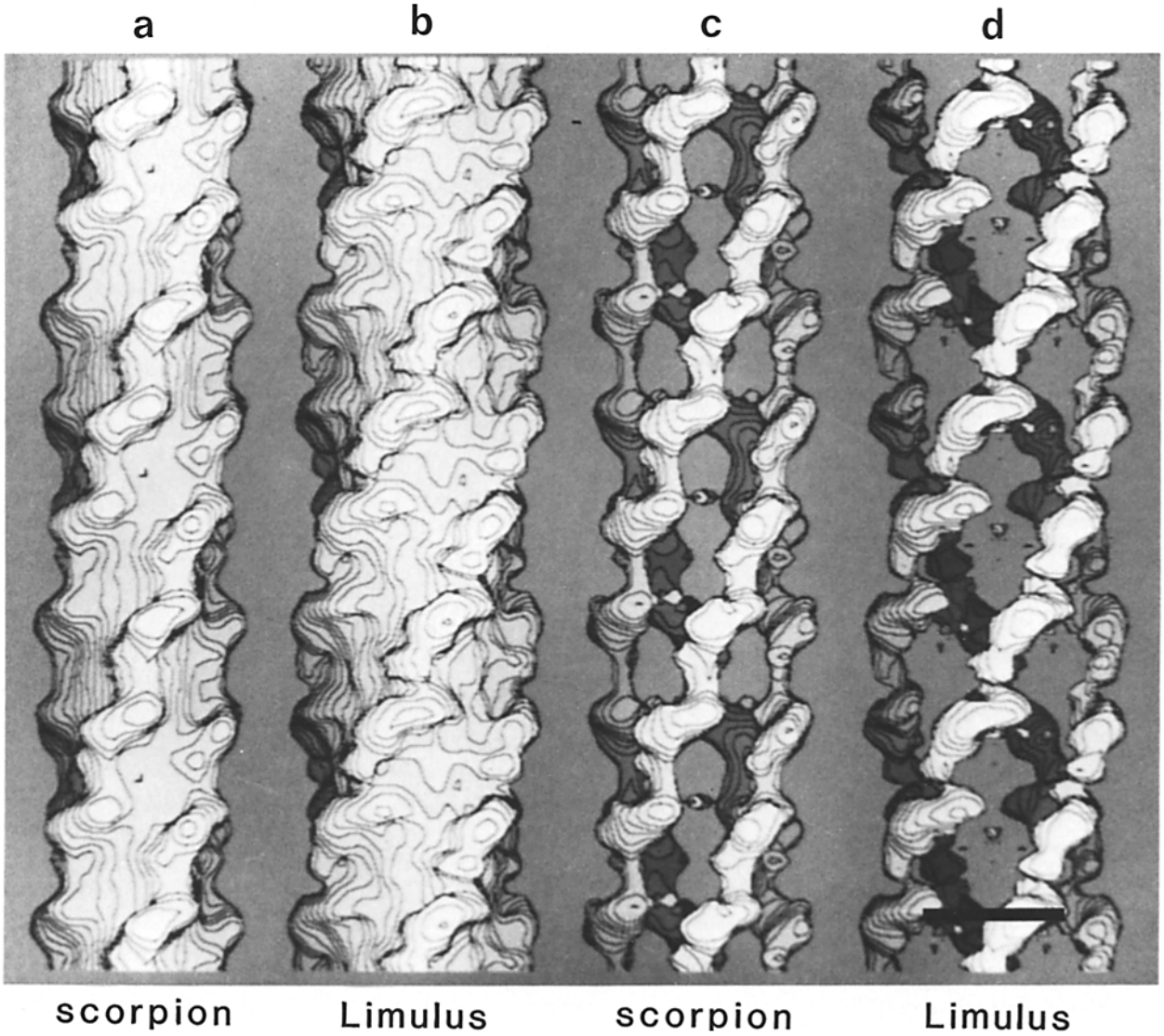

FIGURE 3 Three-dimensional reconstructions of arthropod muscle thick filaments. (*a* and *c*) Scorpion thick filaments. (*b* and *d*) *Limulus* thick filaments. The equatorial data have been included in *a* and *b* but omitted from *c* and *d*. A computer graphics procedure has been employed to give the impression of a solid model viewed from a direction normal to the filament axis. The projecting subunits have a distinct bilobed appearance, with a less dense strand connecting adjacent subunits. The projecting subunits have an approximate dyad appearance so that it is not easy to determine the polarity of the filament without close inspection. The reconstructions are oriented so that the bare zone is at the bottom. Bar, 20 nm.

appeared to be slightly more elongated than their counterparts. Furthermore, the distance between the centers of mass of the two lobes in the *Limulus* projecting subunit was 7 nm, as compared with 5 nm for scorpion. However, the distance between the center of mass of the leading lobe of one subunit and the trailing lobe of the next was ~10 nm, which was essentially the same as that observed in the scorpion. The center of mass of the subunits was at a radius of ~15–16 nm. The angle of these projecting subunits to the 174 nm long-pitch helix was about 15°, somewhat lower than that observed on scorpion filaments. The narrow segment linking successive projecting subunits along the 174 nm long-pitch helix was also slightly different in the *Limulus* reconstructions and contained an additional minor lobe almost midway between the projecting subunits, which, in Figs. 3 and 4, appeared as a tapering extension of the lower lobe in the projecting subunit. Like the scorpion thick filament, there is a suggestion of a two-fold axis (see particularly Fig. 5 *f*), but this was not so pronounced in the *Limulus* reconstructions.

DISCUSSION

Comparison of the Limulus and Scorpion Reconstructions

The reconstructions of *Limulus* and scorpion thick filaments were quite similar and a large proportion of the variation between them can be accounted for by differences in the radius of the shaft (and so in the radius at which the heads were located) and in the angle made by the projecting subunits with the filament axis. Both reconstructions showed subunits that contained two major lobes whose extensions formed a linkage between successive subunits along a helical track. This is illustrated in Fig. 6. In the scorpion filaments, the extensions to the lobes appeared to be slightly separated, whereas in the *Limulus* reconstructions they appeared to overlap to produce the secondary lobe between the projecting subunits. Thus, the two lobes in the projecting units were remarkably similar, and, furthermore, the lobes were very similar in the two

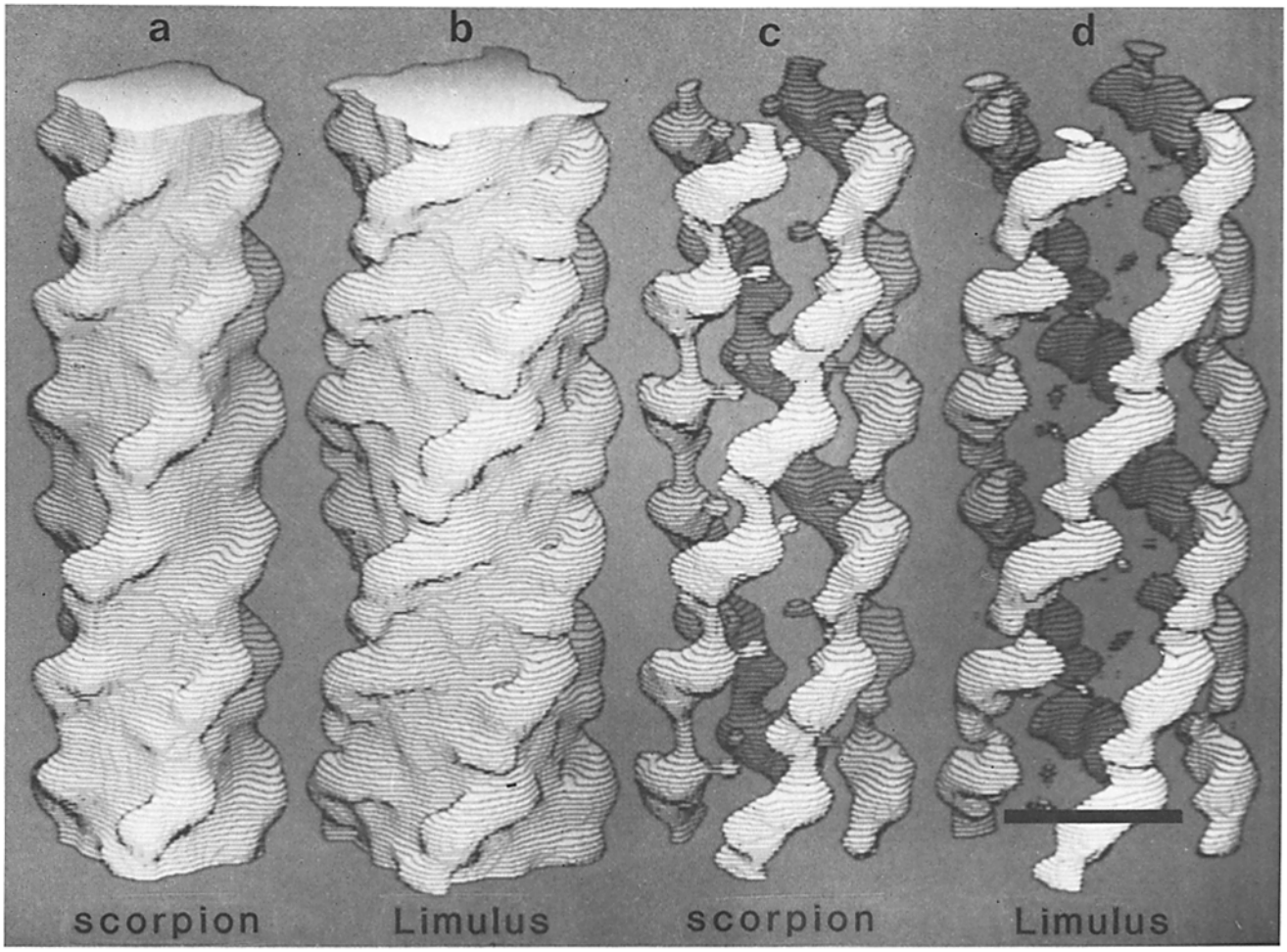

FIGURE 4 Computer model of the reconstructions of arthropod muscles similar to that shown in Fig. 3, but the angle of view is now 70° to the filament axis. (*a* and *c*) Scorpion thick filaments. (*b* and *d*) *Limulus* thick filaments. The equatorial data have been included in *a* and *b* but omitted from *c* and *d*. This view shows how the projecting subunits overlap to form distinct ridges on the filament surface and also illustrates the bilobed appearance of the subunits. The reconstructions are orientated with the bare zone towards the bottom. Bar, 20 nm.

different filaments. Much of the difference in the linkage between projecting subunits observed between the *Limulus* and scorpion filaments can probably be accounted for by a small rotation of the lobes within the projecting subunit. Thus, if both lobes in the scorpion were rotated slightly counterclockwise, the extensions would overlap, essentially as they were observed to do in *Limulus*. In both *Limulus* and scorpion reconstructions there was a strong suggestion of a dyad appearance in the projecting subunit, although in neither case was this absolute.

The observation that these features were not only found independently of whether the equatorial data were included, but were also present in reconstructions of thick filaments from two different species, greatly reinforces our confidence in them as a basis for interpretation.

Location and Orientation of the Individual Myosin Heads

The projecting subunits in both reconstructions were approximately 18 nm long, 8 nm wide, and 6 nm thick. These parameters were not very sensitive to the threshold contour

FIGURE 5 Circumferential sections through the arthropod thick filament reconstructions from which the equatorial data were omitted. Bare zone is towards the bottom. *a–d* are scorpion, whereas *e–h* are *Limulus*. These sections illustrate the division of density within a subunit into two lobes. The bare zone is towards the bottom in each section. The first unbroken contour corresponds to the density threshold employed in Fig. 3. At low radius (10.5 nm in *a* and 13 nm in *e*), the lobe nearest the bare zone is less dense. At radii near the centre of mass of the subunit (12 and 13.5 nm in *b* and *c*, respectively, 14.5 and 16 nm in *f* and *g*, respectively), the two lobes in the subunit are clear and of approximately equal weight. There is a continuous connecting density between projecting subunits. At high radius (15 nm in *d* and 17.5 nm in *h*), the lobe closer to the bare zone is more dense. To enable connectivity between the sections to be more easily appreciated, the horizontal scale has been altered so that features in the four maps of each filament correspond in an azimuthal sense (each spans 180° azimuthally). The vertical scale in each is unchanged. The bar is 10 nm and is correct both horizontally and vertically at the center of mass of the subunit (12.5 nm for scorpion and 15.5 nm for *Limulus*).

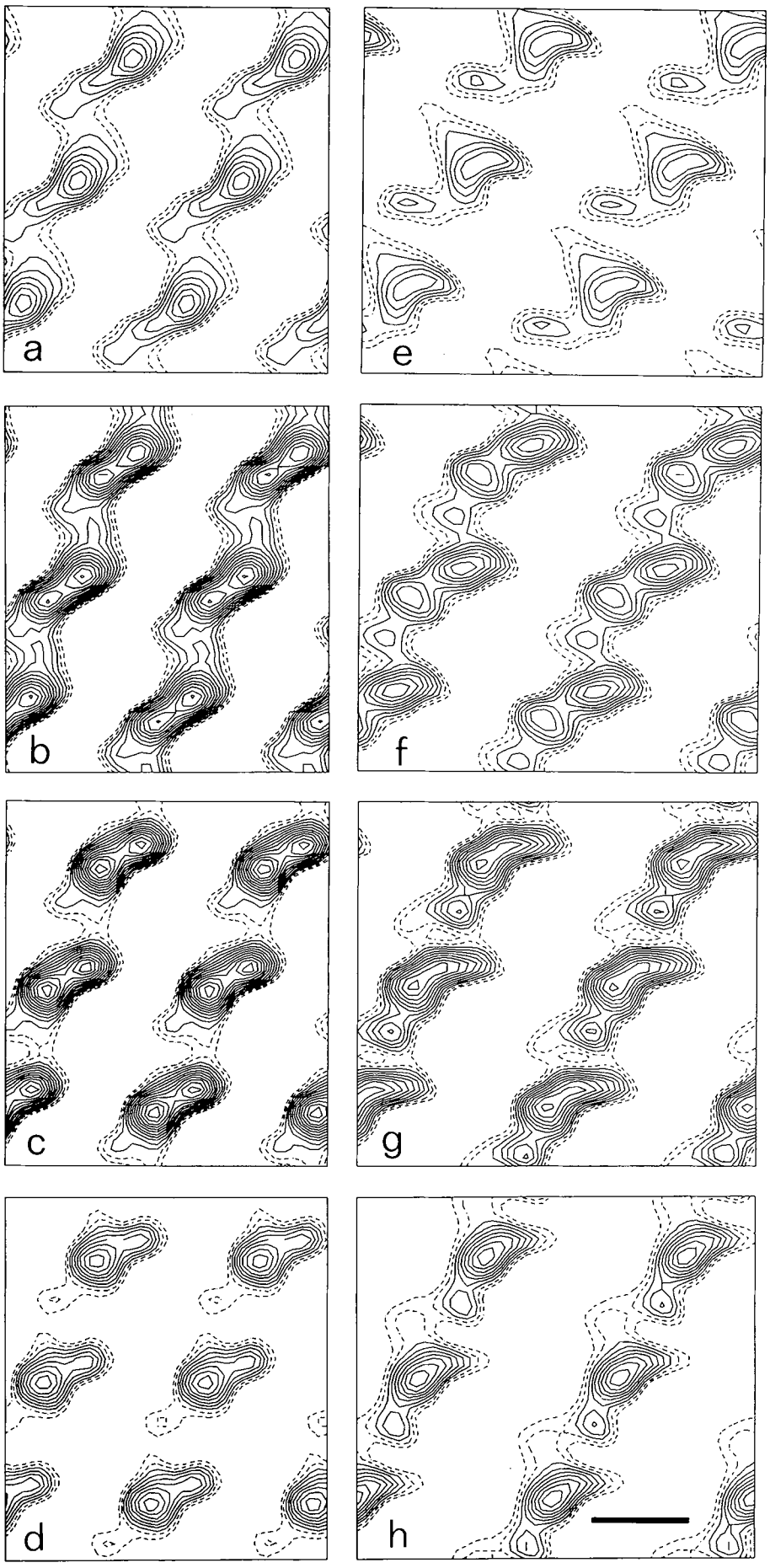
a
e
b
f
c
g
d
h

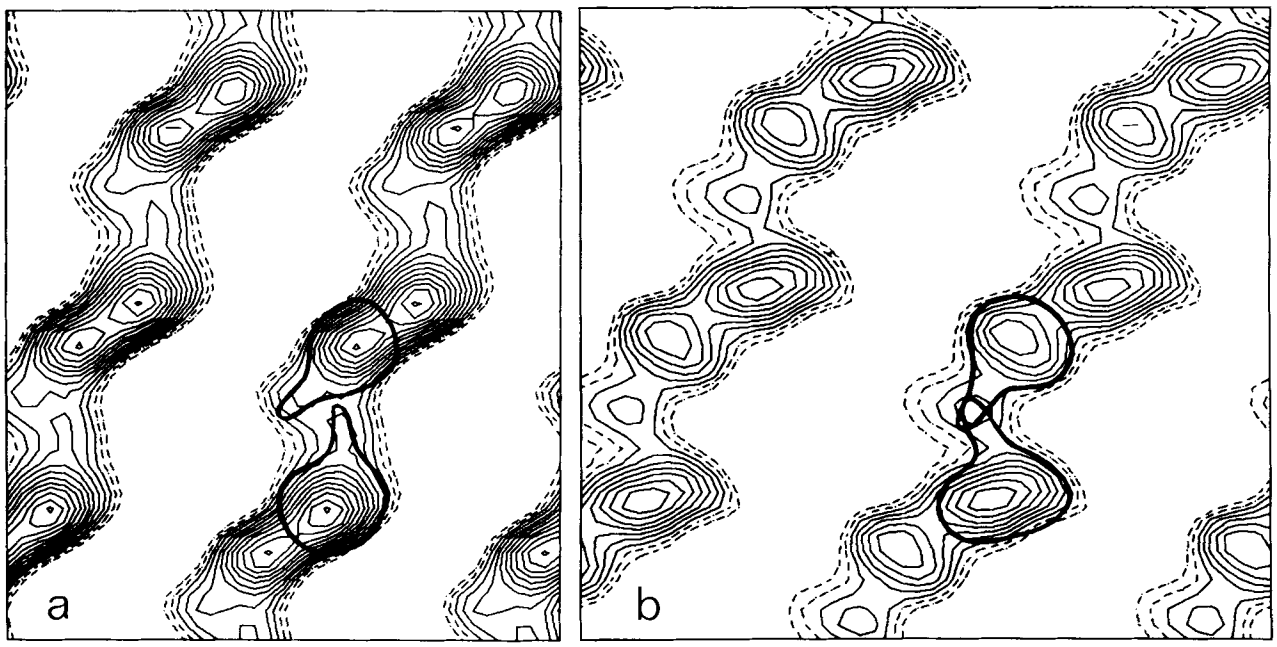

FIGURE 6 Highly schematic illustration of the general outline of the lobes within the repeating subunits of scorpion (a) and *Limulus* (b) thick filaments. The general outline of the lobe with its tapering extension is superimposed on circumferential sections at radii of 12 nm (a) and 14.5 nm (b). A small rotation of the lobes within a projecting subunit could transform the appearance of the scorpion thick filament reconstruction (a) into that of the *Limulus* reconstruction (b). Bare zone is towards the bottom.

chosen, because the density fell off rapidly at the ends of the subunits. The projecting subunits were therefore about double the size expected of a single myosin head. Furthermore, the diameter of the *Limulus* shaft is approximately that expected for one myosin molecule per projecting subunit (24). Because it was therefore unlikely that either *Limulus* or scorpion thick filaments contained more than one myosin molecule (that is, two heads) per projecting subunit, the two lobes of the projecting subunit probably correspond to individual heads. Although there was some overlap between the two heads within a projecting subunit, the very marked division of density seen in cylindrical sections through the reconstruction (Figs. 5 and 6) makes this interpretation compelling. In addition, the general shape of the two lobes, with their approximately spherical major density and tapering extensions, and their equivalence in size strongly supported this interpretation.

Because the heads partially overlap, one cannot unequivocally establish the boundary between them. Therefore, determining their orientation and connectivity was not completely straightforward, although two general interpretations were consistent with the appearance of the reconstructions (see Fig. 7).

In the first (interpretation *A*), the two curved, pear-shaped myosin heads in a projecting subunit would be arranged antiparallel. This would account for the presence of approximate dyad axes at the center of each subunit. The narrow bridge between subunits would represent the ends of the myosin heads that taper towards their junction with the rod portion of the molecule (Fig. 7). This junction would probably be near the midportion of the linker unit, where there is a small increase in density in both scorpion and *Limulus* reconstructions. In interpretation *A*, the two heads in each projecting subunit derive from different myosin molecules. This was, perhaps, unexpected, as one tends to associate the projecting subunits in the reconstructions with myosin molecules. However, the size (approximately 16 × 5 × 5 nm) and shape of the heads in this interpretation are not unrealistic. It is interesting that Haselgrove (9) proposed that an arrangement of myosin heads similar to that in interpretation *A* was necessary to account for the low-angle x-ray diffraction pattern from relaxed frog sartorious muscle and this orientation has also been tentatively suggested for tarantula thick filaments (22). Interpretation *A* agrees well with the scorpion reconstructions, in which the connecting span was approximately the same size at both the top and bottom of the subunit and the dyad appearance was clearer. We can reasonably reconcile interpretation *A* with the *Limulus* reconstruction by proposing that the lower extension of the subunit represents an overlap of the two tapering "stalks" of the myosin heads and that the stalks are at slightly different radii or have different conformations so that the stalk attached to the trailing lobe in the subunit appeared more dense in the reconstructions. This was not unreasonable, since the center of mass of the trailing lobe was at a slightly higher radius than the leading lobe.

The second interpretation (*B*) proposes that the two heads in a subunit would be arranged parallel, with one head overlapping the other as illustrated in Fig. 7. Both heads would be curved and pear-shaped, and the underlying head would extend further towards the Z-line. In the *Limulus* reconstruction, the tapering extension at the bottom of the projecting subunit (that is, closer to the bare zone) would represent the tapering stalks of the two heads. However, in the scorpion reconstruction there is little polarity in the linkage between projecting subunits.

A third but less likely interpretation would be that the antiparallel heads in a subunit derived from the same molecule, in which case the heads would be connected at the center of the subunit. The linkers between subunits would represent either tapering domains at the end of the heads distal to the junction with the rod or, alternatively, part of the head that then doubled back underneath itself to join to the rod. However, because in both cases the shape of the heads would be

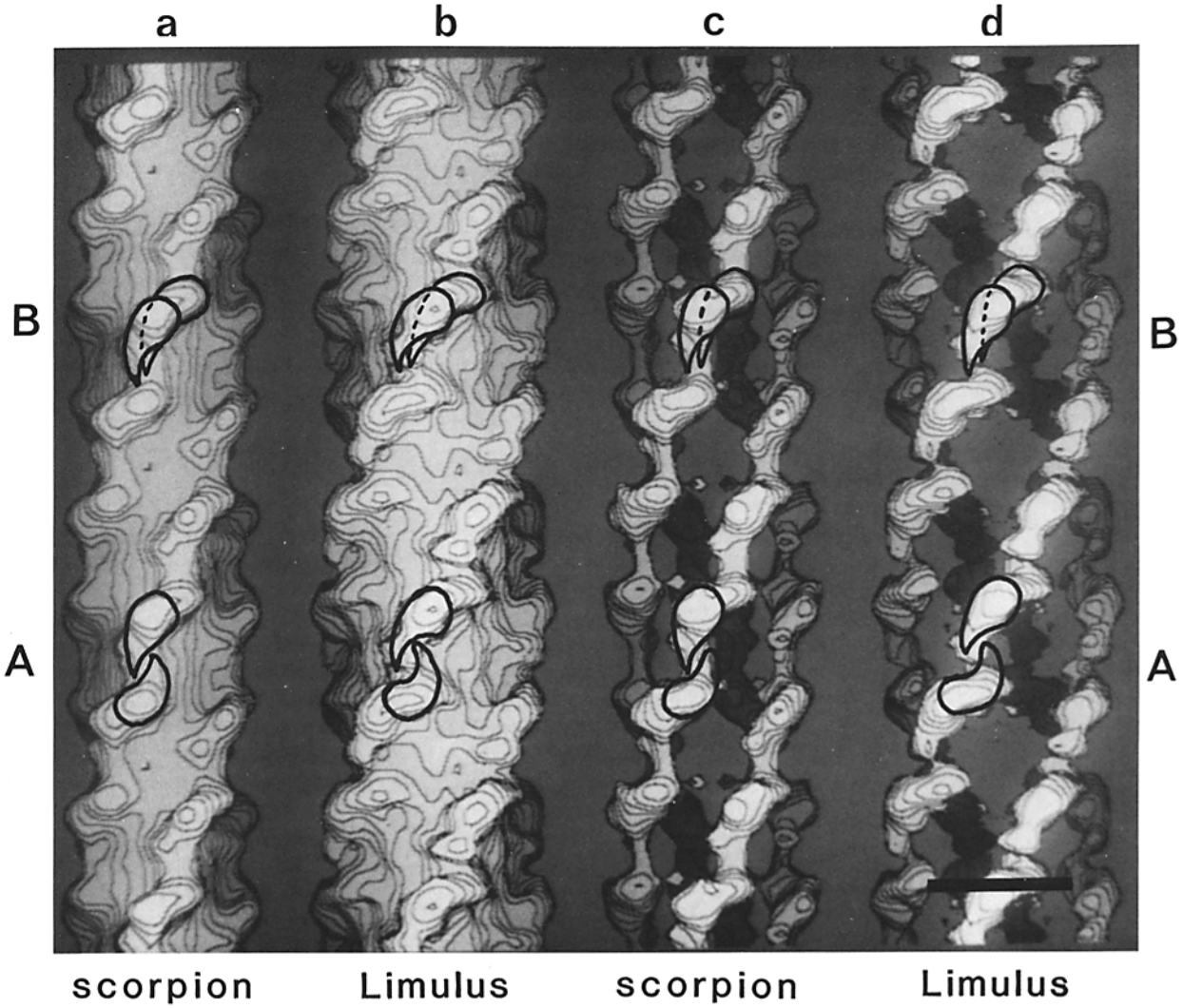

FIGURE 7 Illustration of possible interpretations of the reconstructions in respect to individual myosin head positions and orientations. Bare zone is towards the bottom. In interpretation *A* (at the middle of each filament) the two heads in the subunit are antiparallel and probably derive from different myosin molecules, whereas in interpretation *B* (at the top of each filament), both heads are parallel and point away from that bare zone. There are a number of indications, discussed in the text, that suggest that interpretation *A* is more likely. Because of the overlap between heads, it was impossible at the resolution of this study to determine exact boundaries unequivocally, and so the outlines of the heads drawn on this figure should be considered only as indications of head position in the two different interpretations. Bar, 20 nm.

rather different from that commonly accepted (4), these interpretations are probably incorrect.

The subunit shape and size in both interpretations *A* and *B* appeared realistic and broadly consistent with other data on the size and shape of the myosin heads. However, the different axial position of the major portion of the heads in interpretation *B* presents a problem. The overlying molecule usually appeared to be shorter than the underlying one, whereas the two myosin heads should be identical. Interpretation *A*, however, was easily reconciled with both reconstructions and had both heads being of essentially the same size. Furthermore, in this interpretation both the light chains, which are thought to be located mainly near the junction of the heads with the tail (6), would be on the filament surface and so relatively exposed. By contrast, in interpretation *B*, the light chain of the underlying head would probably be obscured to some extent by the overlying head. Because the state of light chain phosphorylation, in conjunction with thin filament Ca-sensitive proteins, controls contraction in *Limulus* muscle (23), it may be important for the light chain to be easily accessible to kinases.

Additional support for interpretation *A* derived from the difference in location of the centers of mass of the lobes within the projection subunits. In scorpion these were separated by ~5 nm, whereas in *Limulus* they were separated by ~7 nm (see Fig. 4, *b* and *f*). This contrasted with the separation between the centers of mass of the leading lobe of one subunit and the trailing lobe of the next, which was ~10 nm in both *Limulus* and scorpion thick filaments. One would expect the separation between heads within a myosin molecule to remain constant, but because they are located at a higher radius (and so are more separated circumferentially), one would expect the separation between myosin molecules (and so between heads on adjacent molecules) to be greater in the *Limulus* filaments. Therefore, interpretation *A* would be consistent with the greater separation between the lobes in the *Limulus* projection subunits, whereas interpretation *B* (in which both heads in the projecting subunit derive from the same mole-

cule) would not account for this difference.

Overall we prefer interpretation *A*, although interpretation *B* probably cannot be excluded on the basis of the available data. Tarantula thick filament reconstructions (2, 22) also favor interpretation *A*. We attempted to obtain direct evidence for the positioning of the heads by examining the appearance of filaments near the bare zone. If the molecular packing were not altered at the bare zone, interpretation *A* would predict that the last line of projecting units should have half weight, whereas interpretation *B* would predict that the last line of subunits should have full weight. Unfortunately, the patterns in either negatively stained or shadowed filaments were not sufficiently clear to enable an unequivocal decision to be made. Since interpretation *B* places heads from the same molecule nearby, whereas interpretation *A* places heads from different molecules next to one another, it may be possible to distinguish between these interpretations by chemical methods, such as cross-linking.

Despite extensive studies, it has not been possible to demonstrate interactions between the two heads within a myosin molecule. However, there is evidence that individual S-1 heads do dimerize to an extent in solution, particularly at higher protein concentrations (5, 21). Because the S-1 heads are thought to dimerize end-to-end (21), they may be prevented from interacting within a myosin molecule by virtue of their attachment to the rod. A striking feature of the reconstructions obtained here is the compact and ordered packing of the myosin heads on the filament surface. This would be consistent with an interaction between heads, which could easily be the same in both filament types even though the overall position of the heads is slightly different. In the case of interpretation *A*, this interaction would be between heads of different myosin molecules and might possibly represent an interaction between heads similar to that observed between isolated S-1 units in solution. This might account for the similarity in appearance of the projecting subunits in arthropod muscle thick filaments that have different shaft radii and paramyosin contents and so, presumably, different shaft structures (see reference 13).

Myosin Head Size and Shape

There are a number of observations about the shape, size, and orientation of the heads that would be true for either interpretation *A* or *B*.

The myosin heads are distinctly curved in both interpretations, and this agrees both with observations on isolated molecules (3) and with three-dimensional reconstructions of decorated thin filaments (20, 25, 26, 28) and scallop thick filaments (27). The heads also have a pearlike shape in both interpretations, as originally proposed by Elliott and Offer (4). This latter feature was most marked in interpretation *A*, where the heads tended to take on almost a comma shape (see reference 6). There is little evidence for domain structure in the scorpion reconstruction, except that there appeared to be a subsidiary density in the tapering portion of the head near the junction with the tail. This can be seen both on the solid models and in sections through the reconstruction and may represent light chain material that has been seen in this region of the molecule by other methods (29). The *Limulus* reconstruction also has this feature and, in addition, has a number of protuberances in the thicker distal region of the head, which may indicate the presence of some substructure.

In both interpretations, the heads appear to be ~16 nm long, similar to those observed in scallop thick filament reconstructions (27). A length as great as 18 nm could probably be reconciled with interpretation *B*, whereas in interpretation *A*, the heads would be a little shorter and could probably be reconciled with lengths as low as 14 nm. The exact size of a myosin head is controversial, but the estimate of ~16 nm from the present study is within the range of values usually quoted. Electron micrographs of shadowed myosin molecules were originally taken to indicate a pear-shaped head ~19 × 5 nm (4). However, since the volume of these heads appears higher than expected on the basis of molecular weight, they may have been distorted by the preparative procedures employed. Alternatively, x-ray solution studies (18, 19) indicate a maximum chord length in S-1 of 12 nm, which would be consistent with a contour length of only ~13–14 nm. Reconstructions of decorated thin filaments (25, 26, 28) support a similar length, although difficulties in establishing molecular boundaries at high radii mean the lengths from these studies should be considered as only a minimum. The heads in the *Limulus* and scorpion reconstructions are thus shorter than those seen in shadowed material but longer than indicated by solution x-ray scattering.

Another feature common to both interpretations is that the heads would not be in equivalent orientations relative to the thick filament axis. This difference would be substantial in interpretation *A* and present, although less marked, in interpretation *B*. When some fluorescence and electron paramagnetic resonance probe data and also some x-ray diffraction data from muscle are interpreted, it is usually assumed that the two heads of each myosin molecule have equivalent orientations. Our results suggest that this may not be correct and raise the possibility, for example, that some data that have been taken to suggest a rather random orientation of heads in relaxed muscle might be open to reinterpretation.

Some electron paramagnetic resonance probe studies (for example, reference 1) have indicated that essentially all myosin heads in relaxed muscle are highly mobile, whereas the results we have obtained here indicate a much more ordered arrangement of the heads. There was probably disorder corresponding to a root mean square displacement of ~1 nm in the negatively stained filaments we investigated (and this was probably a major cause of the limitation of resolution to 5 nm), but the displacement was much less than that indicated by the probe work. Because the volume of the projecting subunits was near that expected for two myosin heads, it is unlikely that part of the head was disordered and so obscured in our reconstructions. Because of the close correspondence between the optical diffraction patterns of our negatively stained filaments and x-ray diffraction patterns of relaxed muscle (30–32), it was unlikely that we had introduced order into our specimens. Also, the degree of order in x-ray diffraction patterns of relaxed frog and *Limulus* muscles appears to be similar. Thus we cannot presently account for the degree of mobility indicated by the probe results.

We are most grateful to our colleagues in Cambridge and Philadelphia, particularly Drs. R. A. Crowther, H. E. Huxley, A. Klug of the MRC Laboratory of Molecular Biology, Cambridge, and A. P. Somlyo of the Pennsylvania Muscle Institute, Philadelphia, for their many helpful comments and criticisms. We are indebted to Dr. R. A. Crowther for many detailed discussions and for showing us his three-dimensional reconstructions of tarantula thick filaments. We thank

Drs. R. A. Crowther, E. H. Egelman, A. Lesk, and T. S. Horsnell of the MRC Laboratory of Molecular Biology for computer programs and for advice on their use. This work was supported in part by U. S. Public Health Service grants AM30442 to R. W. Kensler and HL15835 to the Pennsylvania Muscle Institute.

Received for publication 3 December 1984, and in revised form 8 April 1985.

REFERENCES

1. Barnett, V. B., and D. D. Thomas. 1984. Saturation transfer electron paramagnetic resonance of spin-labeled muscle fibres. *J. Mol. Biol.* 179:83–102.
2. Crowther, R. A., R. Padron, and R. Craig. 1985. Three dimensional structure of tarantula thick filaments. *J. Mol. Biol.* In press.
3. DeRosier, D. J., and P. Moore. 1971. Reconstruction of three-dimensional images from electron micrographs of structures with helical symmetry. *J. Mol. Biol.* 52:355–369.
4. Elliott, A., and G. Offer. 1978. Shape and flexibility of the myosin molecule. *J. Mol. Biol.* 123:505–509.
5. Flaming, D. P., and M. A. Cusanovich. 1981. Aggregtion-linked heterogeneity in bovine cardiac myosin subfragment I. *Biochemistry.* 20:6760–6767.
6. Flicker, P. F., T. Walliman, and P. Vibert. 1983. Electron microscopy of scallop myosin—location of regulatory light chains. *J. Mol. Biol.* 169:723–741.
7. Fraser, R. D. B., and T. P. MacRae. 1973. Conformation in Fibrous Proteins. Academic Press, Inc., New York. 628 pp.
8. Hardwicke, P. M. D., and J. Hanson. 1971. Separation of thick and thin myo-filaments. *J. Mol. Biol.* 59:509–516.
9. Haselgrove, J. C. 1980. A model of myosin cross-bridge structure consistent with the low-angle X-ray diffration pattern of vertebrate muscle. *J. Muscle Res. Cell Motil.* 1:177–191.
10. Kensler, R. W., and R. J. C. Levine. 1982. An electron microscopic and optical diffraction analysis of the structure of *Limulus* telson muscle thick filaments. *J. Cell Biol.* 92:443–451.
11. Kensler, R. W., and R. J. C. Levine. 1982. Determination of the handedness of the crossbridge helix of *Limulus* thick filaments. *J. Muscle Res. Cell Motil.* 3:349–361.
12. Kensler, R. W., and M. Stewart. 1983. Frog skeletal muscle thick filaments are three stranded. *J. Cell Biol.* 96:1797–1802.
13. Kensler, R. W., R. J. C. Levine, and M. Stewart. 1985. An electron microscope and optical diffraction analysis of the structure of scorpion muscle thick filaments. *J. Cell Biol.* 101:395–401.
14. Klug, A., F. H. C. Crick, and H. W. Wykoff. 1958. Diffraction by helical structures. *Acta Crystallogr.* 11:199–213.
15. Deleted in press.
16. Levine, R. J. C., R. W. Kensler, M. C. Reedy, W. Hofmann, and H. A. King. 1983. Structure and paramyosin content of tarantula thick filaments. *J. Cell Biol.* 97:186–195.
17. McLachlan, A. D., and J. Karn. 1982. Periodic charge distributions in the myosin rod amino-acid sequence match cross-bridge spacings in muscle. *Nature (Lond.).* 299:226–231.
18. Mendelson, R., and K. M. Kretschmar. 1980. Structure of myosin S-1 from low angle X-ray scattering. *Biochemistry.* 19:4103–4108.
19. Mendelson, R., and P. Wagner. 1984. X-ray scattering by single-headed heavy meromyosin. *J. Mol. Biol.* 177:153–171.
20. Moore, P. B., H. E. Huxley, and D. J. DeRosier. 1970. Three-dimensional reconstruction of F-actin, thin filaments and decorated thin filaments. *J. Mol. Biol.* 50:279–295.
21. Morel, J. E., and M. Garrigos. 1982. Dimerisation of the myosin heads in solution. *Biochemistry.* 21:2679–2686.
22. Padrón, R., R. A. Crowther, and R. Craig. 1984. Three-dimensional reconstruction of native tarantula muscle thick filaments. *Biophys. J.* 45(No. 2, Pt. 2):10*a*. (Abstr.)
23. Sellers, J. R. 1981. Phosphorylation-dependent regulation of *Limulus* muscle. *J. Biol. Chem.* 256:9274–2978.
24. Stewart, M., R. W. Kensler, and R. J. C. Levine. 1981. Structure of *Limulus* telson muscle thick filaments. *J. Mol. Biol.* 153:781–790.
25. Taylor, K. A., and L. A. Amos. 1981. A new model for the geometry of the binding of myosin crossbridges to muscle thin filaments. *J. Mol. Biol.* 147:297–324.
26. Vibert, P., and R. Craig. 1982. Three-dimensional reconstruction of thin filaments decorated with a Ca-regulated myosin. *J. Mol. Biol.* 157:299–319.
27. Vibert, P., and R. Craig. 1983. Electron microscopy and image analysis of myosin filaments from scallop striated muscle. *J. Mol. Biol.* 165:303–320.
28. Wakabayashi, T., and C. Toyoshima. 1981. Three dimensional analysis of the complex of thin filaments and myosin molecules from skeletal muscle. II. The multidomain structure of actin-myosin S-1 complex. *J. Biochem. (Tokyo).* 90:683–701.
29. Walzthöny, D., M. Bähler, H. M. Eppenberger, T. Wallimann, and A. Engel. 1984. Unshadowed myosin molecules: STEM mass-maps of myosin heads. *EMBO (Eur. Mol. Biol. Organ.) J.* 3:2621–2626.
30. Wray, J. S. 1982. Organisation of myosin in invertebrate thick filaments. *In* Basic Biology of Muscle: A Comparative Approach B. M. Twarog, R. J. C. Levine, and M. M. Dewey, editors. Raven Press, New York. 29–36.
31. Wray, J. S., P. J. Vibert, and C. Cohen. 1974. Crossbridge arrangements in *Limulus* muscle. *J. Mol. Biol.* 88:343–348.
32. Wray, J. S., P. J. Vibert, and C. Cohen. 1975. Diversity of crossbridge arrangements in invertebrate muscles. *Nature (Lond.).* 257:561–564.